



Analysis of evolution of seismic components induced by a vertical blasthole

Qidong Gao^{1,2} · Wenbo Lu^{1,2} · Zhaowei Yang^{1,2} · Peng Yan^{1,2} · Ming Chen^{1,2}

Received: 29 January 2018 / Accepted: 22 November 2018 / Published online: 3 December 2018
© Springer-Verlag GmbH Austria, ein Teil von Springer Nature 2018

Abstract

Blast ground vibration is the integrated result of body waves and surface waves. However, the contribution of various waves and their evolution laws have not been well studied, and the concept of the influence areas of various waves is rarely mentioned in current studies. In this paper, using the polarization analysis approach, the seismic components and the evolution of various waves induced by a vertical blasthole are analyzed in two case studies. Then, based on the test results, the partition of the influence areas of various waves is discussed. The results indicate that the proportion of different seismic components is not a constant, but rather, the dominant wave may change to another type with r (where r is the distance to the blasthole axis), and the dominant motion directions of various waves are distinct. For a vertical blasthole, the P-wave is a significant component in both near and far fields, and becomes the dominant wave beyond $r=2.3 h$ (where h is the buried depth of the explosive), furthermore its particle motion gradually rotates to the horizontal direction with r increases. The S-wave only dominates within $r=2.3 h$, but its effect can be ignored when the R-wave is well developed. The R-wave is not suddenly created but gradually grows to an identifiable feature at $r=5 h$, and it dominates the vertical vibration if r exceeds $(43 \sim 45)h$ ($59 \sim 62 \text{ m/kg}^{1/2}$). Thus, the P-wave is a non-negligible threat to ground structures in vertical-hole blasting. Nevertheless, the P-wave component is commonly ignored in earthquakes, where the S- and R-waves are considered troublesome. The evolution of seismic components induced by blasting has some differences from the expectations in earthquakes.

Keywords Blast vibration · Vertical blasthole · Seismic components · Evolution laws · Influence areas

List of symbols

| | |
|-----------|--------------------------------|
| λ | Bulk modulus |
| μ | Shear modulus |
| ν | Poisson's ratio |
| ρ | Medium density |
| C_P | Travel speed of the P-wave |
| C_S | Travel speed of the S-wave |
| C_R | Travel speed of the R-wave |
| u | Horizontal displacement |
| w | Vertical displacement |
| r | Distance to the blasthole axis |

| | |
|-----------|---|
| h | Buried depth of the explosive below the ground surface |
| φ | Angle between the radiation direction and blast-hole axis |

Abbreviations

| | |
|------------------|--------------------------------------|
| P-wave | Longitudinal wave |
| S-wave | Transverse wave |
| R-wave | Rayleigh wave |
| PPV | Peak particle velocity |
| PPV _P | PPV in the P-wave |
| PPV _S | PPV in the S-wave |
| PPV _R | PPV in the R-wave |
| PPV _H | Horizontal PPV |
| PPV _V | Vertical PPV |
| VoD | Explosive velocity of the detonation |
| FEM | Finite element method |
| EoS | Equation of state |
| JWL | Jones-Wilkens-Lee parameters |
| PCL | Chapman-Jouguet pressure |

✉ Wenbo Lu
wblu@whu.edu.cn

¹ State Key Laboratory of Water Resources and Hydropower Engineering Science, Wuhan University, Wuhan 430072, China

² Key Laboratory of Rock Mechanics in Hydraulic Structural Engineering Ministry of Education, Wuhan University, Wuhan 430072, China

1 Introduction

It is well known that the total energy released by explosives is never entirely used for rock fragmentation, and much of the energy is spent in the forms of ground vibration, air blasts, flying rocks, etc. (Hagan 1979; Khandelwal and Singh 2007; Kuzu 2008). Among all the ill effects, the blast vibration is always regarded as the major concern (Khandelwal 2010; Verma and Singh 2013). The prediction, assessment and control of blast vibration always remains a pressing issue in the past, present and future. The three following parameters of the blast vibration are usually used to describe the degree of shaking (Singh et al 2008): peak particle velocity (PPV), frequency and duration. Then, many studies on the prediction methods of PPV have emerged, including the charge weight scaling law and waveform superposition method (Blair 2011a; Yan and Yuen 2015), or the techniques of artificial neural network (Khandelwal and Singh 2009, 2013; Álvarez-Vigil 2012). As the response of the structure subjected to the blast vibration is frequency-dependent (Dowding 1985), many researchers have also investigated the frequency characteristic of blast vibration (Ozer 2008; Singh and Roy 2010; Yang et al. 2016; Zhou et al. 2016). As a result, the frequency-based PPV criterion has been adopted in many regulations. The blast ground vibration is the integrated result of the longitudinal wave (P-wave), transverse wave (S-wave), and Rayleigh wave (R-wave) (Dowding 1996). However, the contribution of various waves and their evolution laws have not been well studied, and the concept of the influence areas of various waves is rarely mentioned in current studies. The blast vibration will be undoubtedly better controlled if the wave type is taken into account. Thus, it is imperative to make a detailed analysis of the evolution of seismic components induced by blasting.

The pioneer studies mainly focused on the seismic radiation from a spherical or cylindrical explosive source (Yi et al. 2016). Favreau (1969) provided the analytical solution of a spherical pressurized cavity, and his solution indicates that only P-wave is beamed out by the spherical charge. Graff (1975) proved that only P-wave is generated from a cylindrical pressurized cavity of infinite length, which is not right for the finite explosive velocity of the detonation (VoD). Heelan (1953) calculated the displacement solution of a short column source in an infinite medium, and declared that both the P- and S-waves are of primary origins that are simultaneously radiated from a finite length of charge. Jordan (1962) and Abo-Zena (1977) subsequently criticized that the Heelan solution has some mathematical inaccuracies. However, White (1983) noted that the Heelan and Abo-Zena solutions

are equivalent in the far field. Blair (2007) also tested the range of validity of the Heelan solution by a scale-independent full-field model. For an extended charge, the solutions can be summed along the entire length of the column, if the contribution of each short element is delayed according to the VoD (Blair and Minchiton 1996). Blair (2010) made a detailed analysis of the seismic radiation from an explosive column. Various experiments were also conducted to investigate the seismic waves generated by cylindrical charges (Vanbrabant et al. 2002; Triviño et al. 2009, 2012). In addition, Gao et al. (2017) made a brief review of the recent numerical simulation approaches, and evaluated the effects of several typical numerical methods in simulating the blast-induced seismic waves.

This paper is an attempt to analyze the evolution of seismic components induced by a vertical blasthole (see Fig. 1). First, using the polarization analysis approach, the seismic components and evolution of various waves induced by a vertical blasthole are analyzed in two case studies. Then, based on the test results, the partition of the influence areas of various waves is discussed. The present work is of great significance to enhance the understanding of blast-induced seismic waves, and improve the prediction and control of blast vibration.

2 Method to interpret the seismic components

2.1 Waves generated by blasting

Different types of seismic waves are generated during blasting. The first type that travels within the medium is known as body waves. The body waves can be divided into the longitudinal wave (P-wave), where the particle motion is parallel to the direction of propagation, and transverse wave (S-wave), where the particle motion is perpendicular to the direction of propagation. With respect to the motion

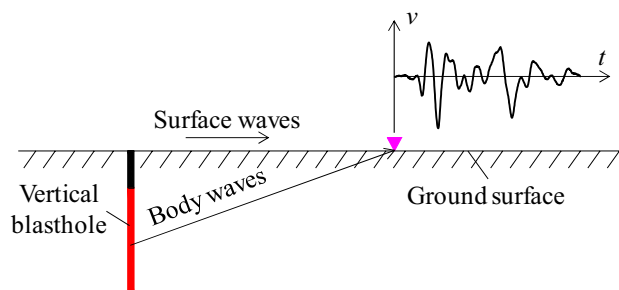


Fig. 1 Illustration of the seismic waves induced by a vertical blasthole

direction of particles, the S-wave can be further divided into horizontally and vertically polarized waves, which are designated as SH and SV, respectively. The second type is named as surface waves because they propagate along the boundary rather than within the interior. It is also called the Rayleigh wave (R-wave), as the existence of surface waves was first predicted by Lord Rayleigh (Whitham 1999). The R-wave is commonly regarded as the coupling of P- and SV-waves (Aki and Richards 2002), and its particle motion near the surface is a retrograde ellipse. Except for the above three types of waves, there are other general types of waves that can be generated by blasting. These include channel waves (via a layer waveguide or a fracture waveguide), Stonely waves (propagating along the interface of different mediums), refracted waves, and Love waves (a type of SH wave). These waves are generated under specific circumstances, so they are not considered in

the present study. In addition, as few SH-wave components are generated by an axisymmetric explosive column, we mainly discuss the P-, SV-, and R-waves in this study. The polarization characteristics of the P-, SV-, and R-waves are illustrated in Fig. 2, based on Bott (1982) and Graff (1975).

2.2 Components interpretation based on the polarization analysis

2.2.1 Prediction of the polarization directions

As mentioned above, the main discrepancies of different waves are the polarization directions and travel speeds in the medium. The seismic components can be interpreted via the polarization analysis approach, as is widely used in Geophysics (Vidale 1986; Park 1987; Blair 1993). To identify the wave components in the collected seismic signal, the polarization directions of different waves must be predicted in advance. Therefore, it is necessary to clarify the relative source-to-site location before interpreting the seismic components. As illustrated in Fig. 3, for the up-going wave (i.e., the seismic source is below the observation point), particles in the P-wave travel in the direction of quadrants 1 and 3, while the S-wave polarizes in the direction of quadrants 2 and 4. For the down-going wave, the particle motion rotates to a perpendicular direction to that in the case of the up-going wave.

2.2.2 Hodogram analysis

An intuitional method to interpret the seismic components is to plot the particle motion trajectory in the displacement coordinates (i.e. Hodogram analysis). Additionally, the arrival time of each wave can also be picked by analyzing the phase difference between the horizontal and vertical vibrations. As the polarization directions of various waves are distinct, the shape of the trajectory change with the arrival of different waves. For example, Fig. 4 illustrates the interpretation of seismic components induced by a vertical-hole blasting. Because the

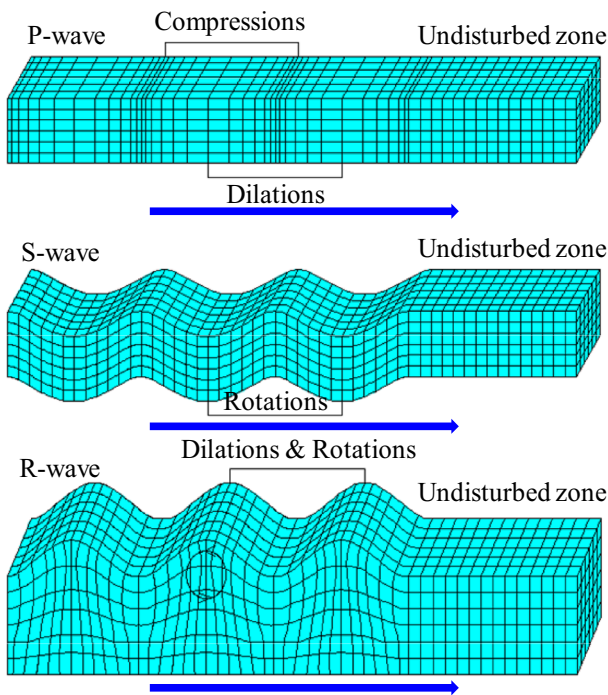
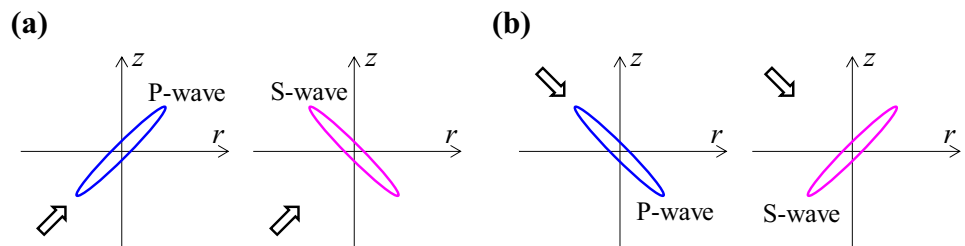


Fig. 2 Illustration of the polarization characteristics of various waves, based on Bott (1982) and Graff (1975)

Fig. 3 Prediction of the polarization directions: **a** up-going wave; **b** down-going wave



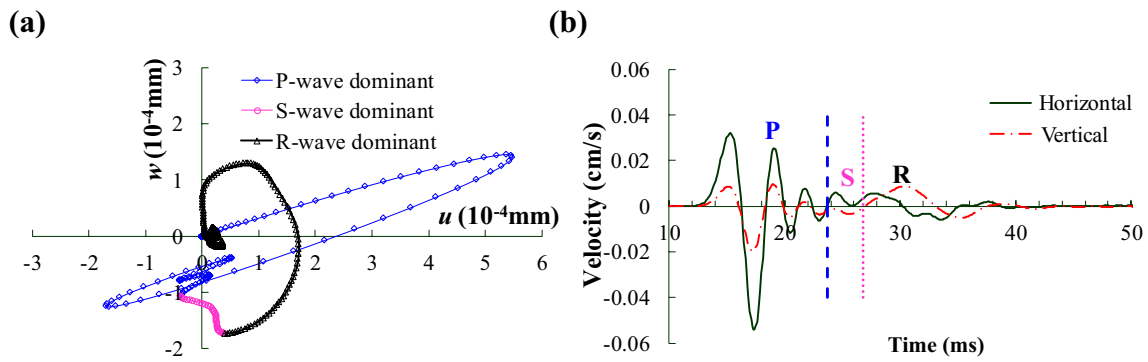


Fig. 4 Illustration of the interpretation of seismic components: **a** particle motion trajectory; **b** comparison of waveforms in the horizontal and vertical directions

trajectory is plotted in time sequence, the arrival time of each wave in the waveform (velocity time-history) is time-corresponded with the variation point of polarization direction in the trajectory.

2.2.3 Procedures to interpret the seismic components

As the recorded blast vibration data is mostly velocity or acceleration time-histories, the displacement time-histories must be calculated by numerical integration of the original data. To obtain the real displacement, the mean value and other distorted signals should be removed by the baseline correction before processing the original data (Hao et al 2001).

To sum up, the procedures to interpret the seismic components can be concluded as follows: (1) Collection of the original data (velocity time-histories); (2) Baseline correction to eliminate the signal irregularities; (3) Numerical integration to obtain the displacement time-histories; (4)

Hodogram analysis; (5) Phase difference analysis; (6) Interpretation of the seismic components.

3 Case study in Baihetan hydropower station

3.1 Site description

The Baihetan hydropower station is located at the border of Ningnan county of Sichuan province and Qiaojia county of Yunnan province in the southwest of China. It is the second step of the four hydropower stations (Wudongde, Baihetan, Xiluodu and Xiangjiaba) in the downstream of Jinsha River. The total installation capacity is 16,000 MW, which is currently the largest capacity under construction in the world. As shown in Fig. 5, a case study with four vertical blastholes was conducted during the foundation excavation of the plunge pool.

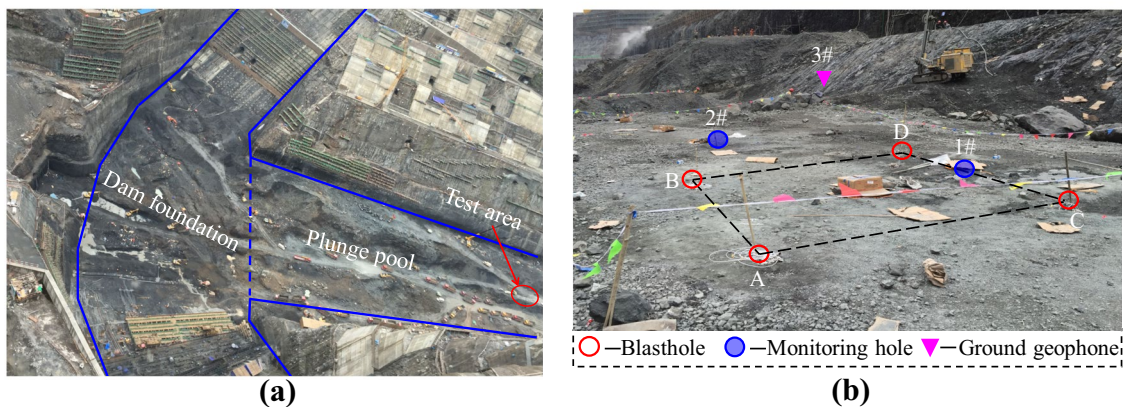


Fig. 5 Site description of the case study in Baihetan hydropower station: **a** location of the test area; **b** onsite layout of blastholes

3.2 Blasting practice and seismic signal acquisition

As shown in Fig. 6a, all blastholes were drilled at four corners of a square, the sides of which are 3.5 m long. Two monitoring holes, numbered as 1# and 2#, were also drilled before blasting, so as to obtain the seismic signal within the rock mass. The installation of geophones 1# and 2# is illustrated in Fig. 6b. Besides, a ground geophone (3#) was placed at 70 m from the center of the square (see Fig. 5b) to monitor the seismic signal at the ground surface. The drilling and blasting parameters are listed in Table 1. The charging structures are plotted in Fig. 7, where blastholes A and B were initiated at the top section of the charge, while blastholes C and D were initiated at the bottom section. All blastholes were fired in the same initiation network, but the non-electric millisecond (MS) detonators were used to delay each blasthole. The delay time is marked in the bracket in Fig. 6a.

Unidirectional transducers (CDJ28), which can monitor the horizontal and vertical vibrations, were installed together in the monitoring hole. The tri-axial transducer, which can synchronously monitor the radial, tangential and

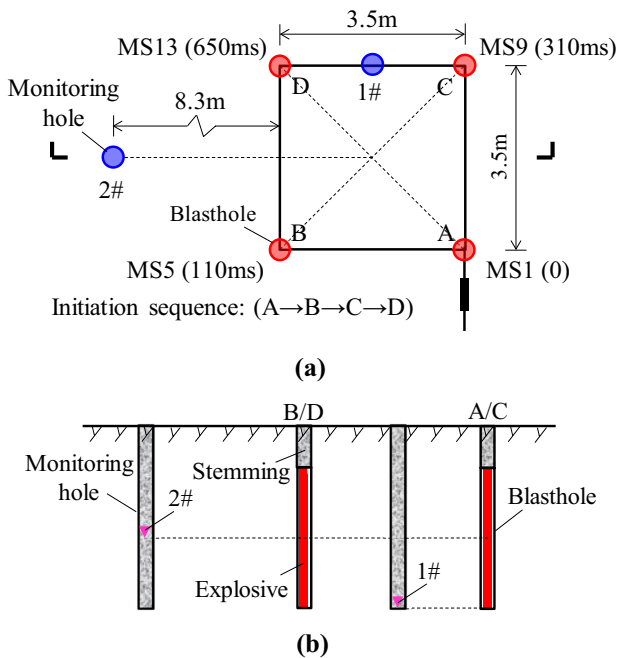


Fig. 6 Layout of the blastholes and set up of the seismic signal acquisition in Baihetan hydropower station: **a** plan view of the blastholes and monitoring holes; **b** cutaway view of the blastholes and monitoring holes

Table 1 Drilling and blasting parameters in Baihetan hydropower station

| Hole diameter | Hole depth | Spacing | Charge diameter | Charge length | Charge weight | Stemming length |
|---------------|------------|---------|-----------------|---------------|---------------|-----------------|
| 100 mm | 6.0 m | 3.5 m | 32 mm | 4.5 m | 4.5 kg | 1.5 m |

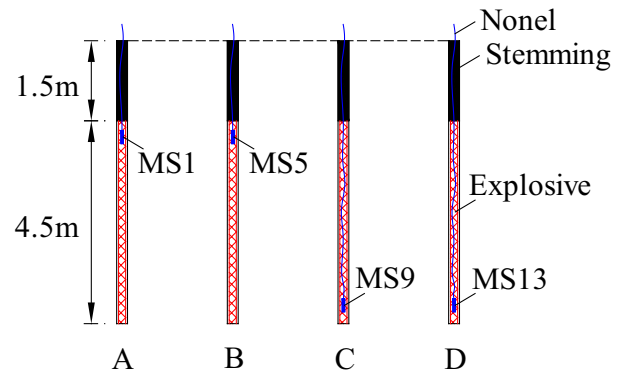


Fig. 7 Charging structures in Baihetan hydropower station

vertical vibrations, was used to monitor the ground blast vibration. The seismograph TC-4850, made in Chengdu Zhongke measurement and control incorporated company in China, was used to record the seismic signal. Figure 8 shows the seismic signal acquisition system in this experiment. Figure 9 plots the typical seismic signal recorded at geophone 2#. Four clear signals are separated in the time axis. The arrival time of each signal is coincident with the designed delay time. They represent the blast vibrations induced by blastholes A, B, C, and D, respectively. To facilitate the description, the blast vibration induced by blasthole A at geophone 1# is numbered as 1#-A hereinafter.

3.3 Test results analysis

3.3.1 Seismic components within the rock mass

Figure 10 shows the typical particle motion trajectories and the associated blast vibration waveforms at geophones 1# and 2#, where u and w denote the horizontal and vertical displacements, and the blue dashed line represents the arrival time of the S-wave. As geophone 1# is located below the explosive center (i.e., down-going wave), the particles in the P-wave travel in the direction of quadrants 2 and 4, while the S-wave polarizes in quadrants 1 and 3. Consequently, the horizontal and vertical vibrations in the P-wave have opposite phases, but those in the S-wave are synchronous. Geophone 2# is located at the same elevation of the explosive center, so the P-wave mainly polarizes in the horizontal direction, while the S-wave oscillates in the vertical direction. Almost no R-wave components can be found, because geophones 1# and 2# are

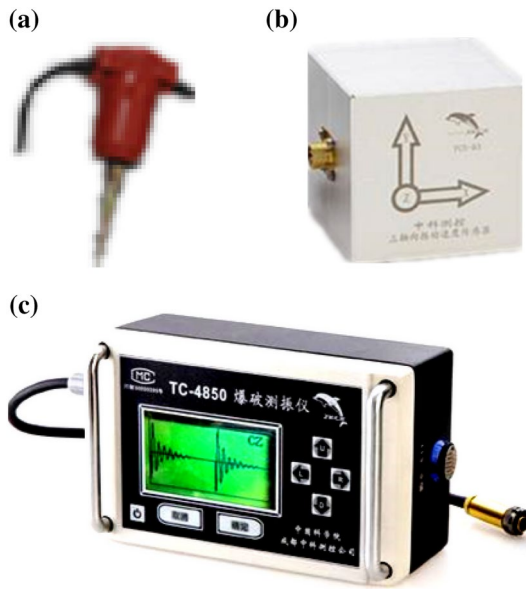


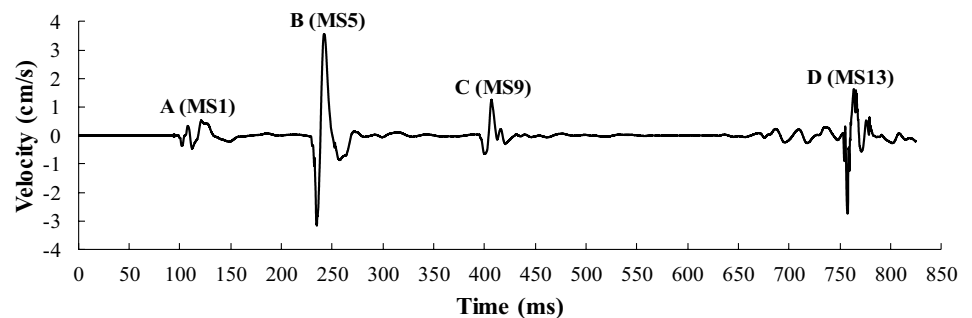
Fig. 8 Seismic signal acquisition system: **a** Unidirectional transducer (CDJ28); **b** tri-axial transducer; **c** seismograph

both located within rock mass, where mainly body waves are included. In addition, geophones 1# and 2# are near the blasting source, where the R-wave is not well developed (Kuzmenko et al. 1993; Aki and Richards 2002).

3.3.2 Seismic components at the ground surface

Figure 11 shows the typical particle motion trajectory and the associated blast vibration waveforms at geophone 3#, where the blue and pink dashed lines respectively represent the arrival time of S- and R-waves. As geophone 3# is located above the explosive center (i.e., up-going wave), particles of the P-wave travel in the direction of quadrants 1 and 3, while those of the S-wave travel in the direction of quadrants 2 and 4. Except for the P- and S-waves, the R-wave, whose particle motion appears to be an anticlockwise ellipse, evidently appears in Fig. 11. In other words, the P-, S- and R-wave components are all included at the ground surface. It

Fig. 9 Typical seismic signals recorded in Baihetan hydro-power station



should be pointed that overlaps among different waves cannot be avoided. The coda of the P-wave is overlapped by the front of the S-wave, and the S-wave is easily overwhelmed by the slightly slower R-wave. Therefore, the letters P, S and R merely represent the dominant wave component in the related time zone. Figure 11 also implies that the S-wave component here is relatively smaller than the P- and R-wave components. This phenomenon will be further discussed in the next case study.

3.3.3 Comparison of PPV induced by P- and S-waves

The PPV values associated with different blastholes are listed in (see Table 4 in Appendix 1). Figure 12 compares the PPV induced by P- and S-waves within the rock mass, where PPV_P and PPV_S are the PPV in P- and S-waves, respectively. It indicates that the contributions of P- and S-waves to the total blast vibration are associated with the motion direction, because all PPV ratios of PPV_S/PPV_P in the vertical direction are relatively larger than those in the horizontal direction. Moreover, the PPV_S/PPV_P ratio varies with the relative source-to-site location, as geophones 1# and 2# are located at different orientations of blastholes A, B, C, and D. Thus, the proportion of P- and S-wave components is not a constant, but varies with the location or orientation.

4 Case study in Fengning pumped storage power station

4.1 Site description

The Fengning pumped storage power station is located at Fengning Manchu Autonomous County of Hebei Province in China. The designed installation capacity is 3600 MW. The construction of the power station is divided into two stages. As shown in Fig. 13, another case study with six vertical blastholes was conducted at the floor of a geology exploration tunnel during the second stage of the project.

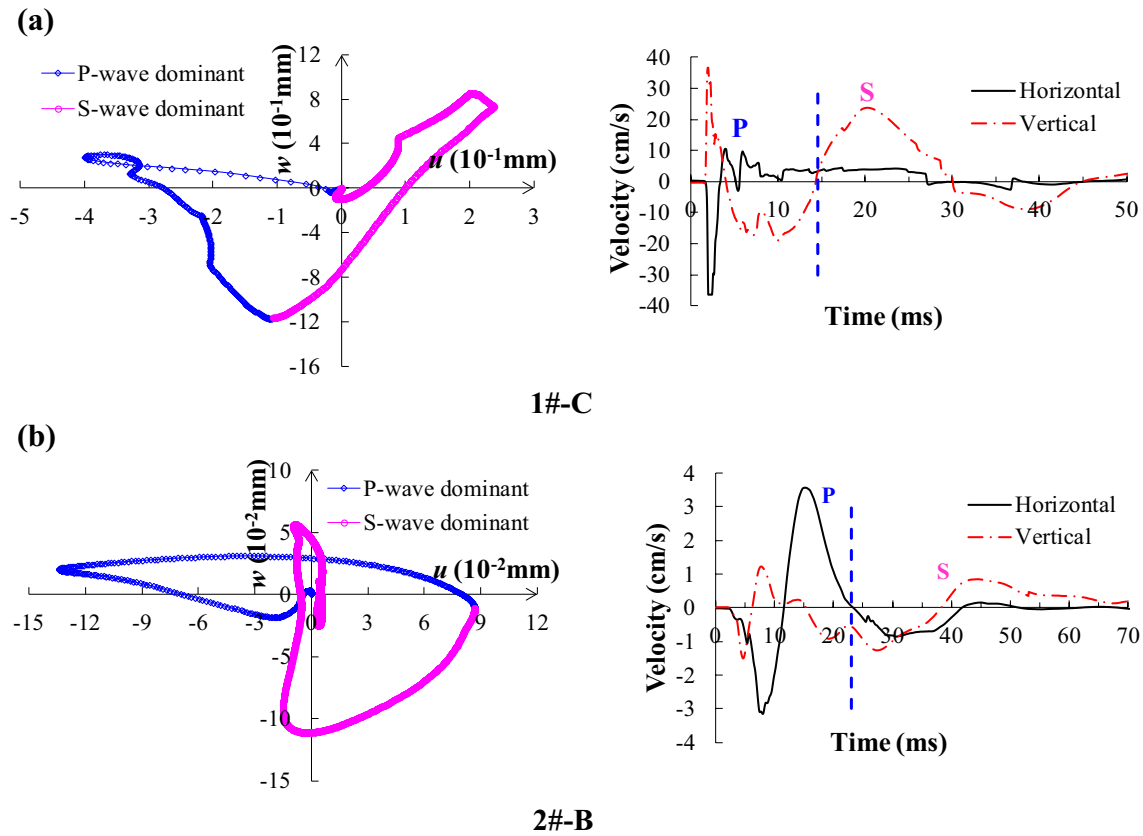


Fig. 10 Interpretation of the seismic components within the rock mass in Baihetan hydropower station: **a** Seismic waves at geophone 1#; **b** Seismic waves at geophone 2#

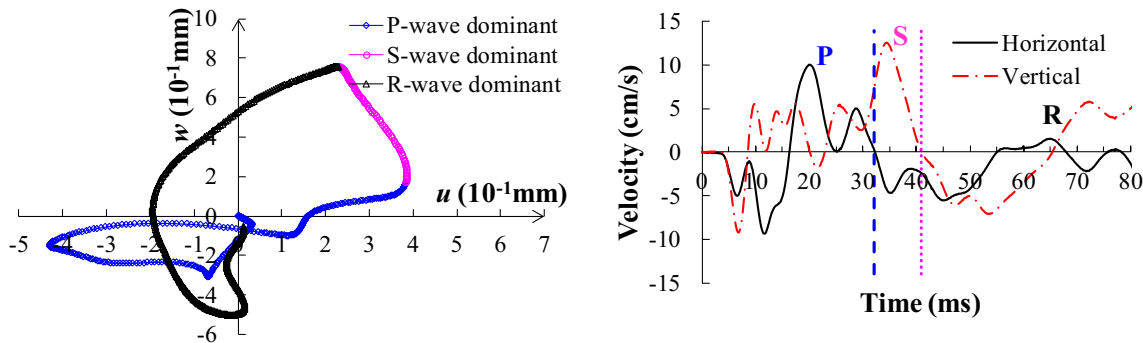


Fig. 11 Interpretation of seismic components at the ground surface in Baihetan hydropower station

4.2 Blasting practice and seismic signal acquisition

As shown in Fig. 14, six vertical blastholes were drilled at the floor of the exploration tunnel. Nine ground geophones were installed and the distance r to the blasthole axis was 13.5–146.0 m. The drilling and blasting parameters are listed

in Table 2. The charging structures are plotted in Fig. 15. All blastholes, which were delayed by the half-second detonator, were fired in the same initiation network, and the initiation sequence is I→II→III→IV→V→VI. Figure 16 plots the typical seismic signal recorded at geophone 1#. Six clear signals are separated in the time axis, which represent the blast vibrations

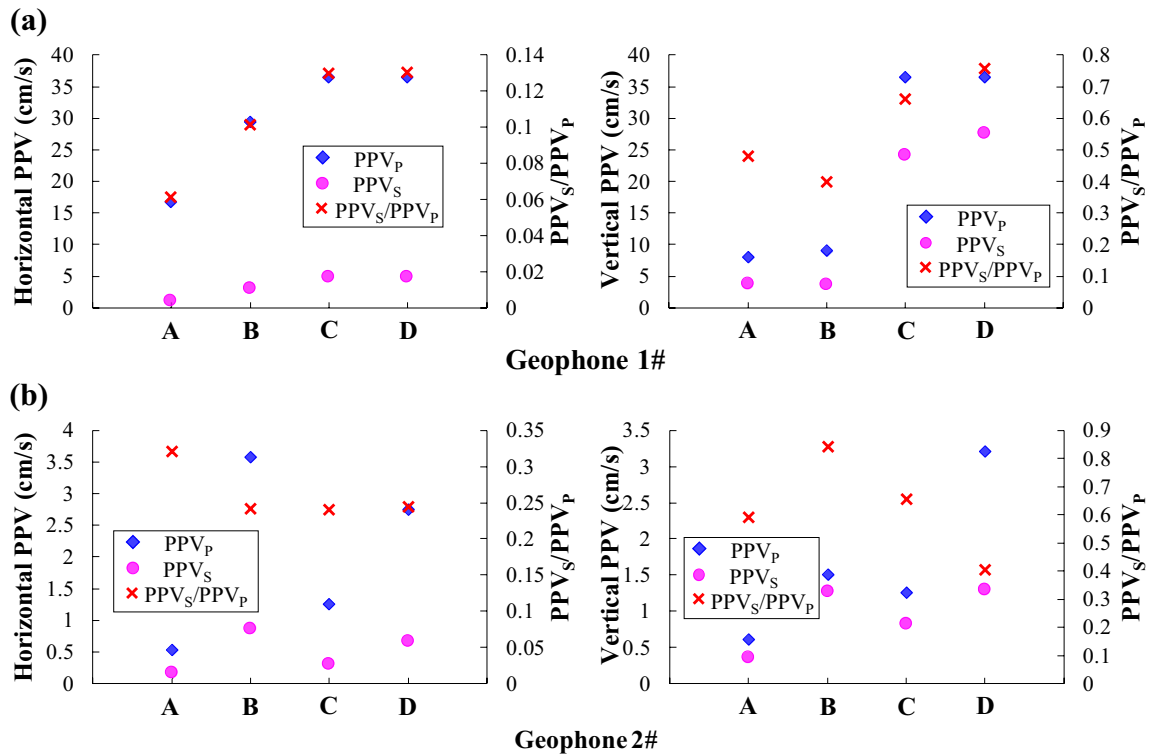


Fig. 12 Comparison of PPV induced by P- and S-waves, where PPV_P and PPV_S are the PPV in P- and S-wave, respectively: **a** PPV recorded at geophone 1#; **b** PPV recorded at geophone 2#



Fig. 13 Site description of the case study in Fengning pumped storage power station: **a** geology exploration tunnel; **b** test area and onsite layout of blastholes

induced by blastholes I, II, III, IV, V and VI, respectively. In this section, blastholes II, IV and VI are selected to analyze the evolution of different waves, as they were fired at the same

location (bottom section of the charge). The buried depths h of the explosive in blastholes II, IV and VI are 5.0 m, 4.0 m and 3.15 m, respectively.

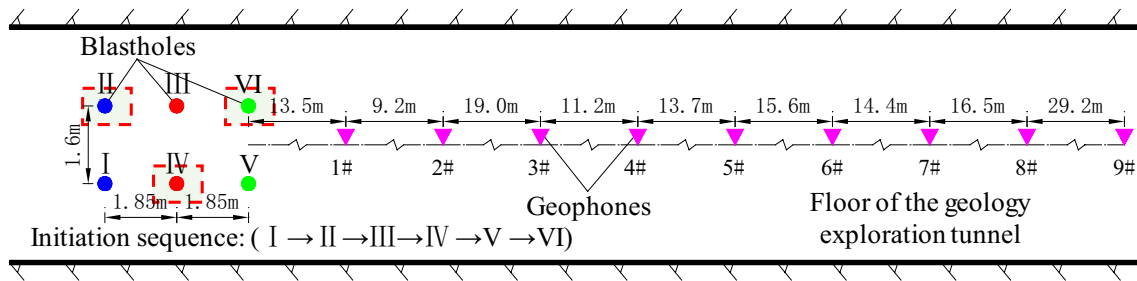
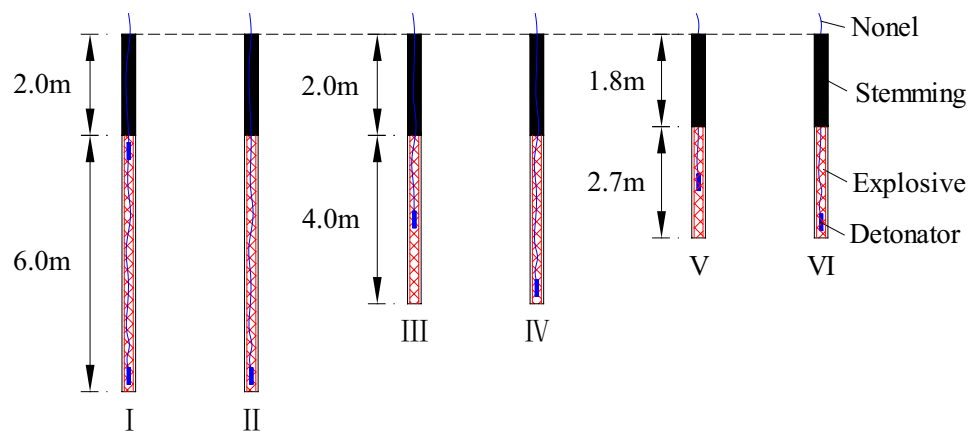


Fig. 14 Layout of the blastholes and geophones in Fengning pumped storage power station

Table 2 Drilling and blasting parameters in Fengning pumped storage power station

| Hole no. | Detonator location | Hole diameter (mm) | Hole depth (m) | Charge diameter (mm) | Charge length (m) | Charge weight (kg) | Stemming length (m) | Buried depth <i>h</i> (m) |
|----------|--------------------|--------------------|----------------|----------------------|-------------------|--------------------|---------------------|---------------------------|
| I | Top/bottom | 76 | 8.0 | 50 | 6.0 | 12.0 | 2.0 | 5.0 |
| II | Bottom | | | | | | | |
| III | Mid-point | 76 | 6.0 | 50 | 4.2 | 8.4 | 1.8 | 4.0 |
| IV | Bottom | | | | | | | |
| V | Mid-point | 76 | 4.5 | 50 | 2.7 | 5.4 | 1.8 | 3.15 |
| VI | Bottom | | | | | | | |

Fig. 15 Charging structures in Fengning pumped storage power station



4.3 Test results analysis

4.3.1 Seismic components analysis

Figure 17 shows the typical particle motion trajectories and the associated blast vibration waveforms at the ground surface. As all geophones are located above the explosive center, particles of the P-wave travel in the direction of quadrants 1 and 3, while those of the S-wave travel in

the direction of quadrants 2 and 4. Figure 17 indicates that the P-, S- and R-waves are all included, but the relative amounts of various waves are distinct. The recorded S-wave component seems to be ignorable when compared to the other two. In addition, this component is easily overwhelmed by the subsequent R-wave. The other typical particle motion trajectories from near to far are also presented in Appendix 2 (see Fig. 25). They indicate that the motion characteristic of various waves varies with *r*,

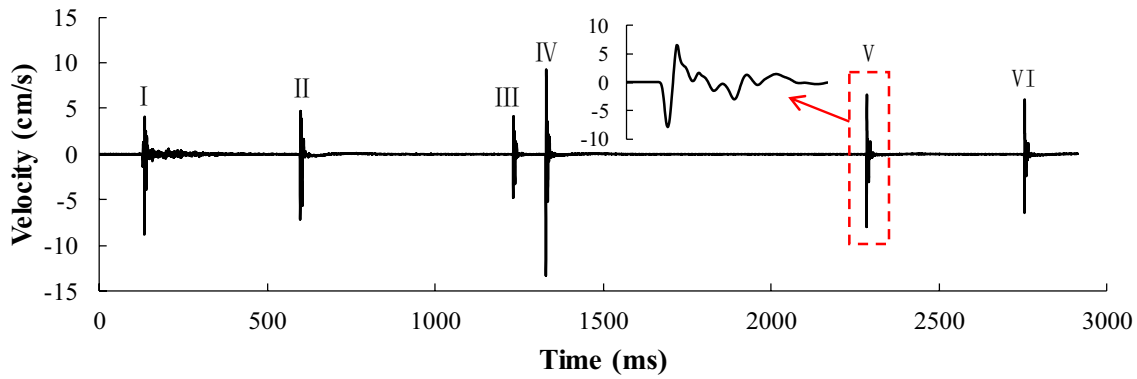


Fig. 16 Typical seismic signals recorded in Fengning pumped storage power station

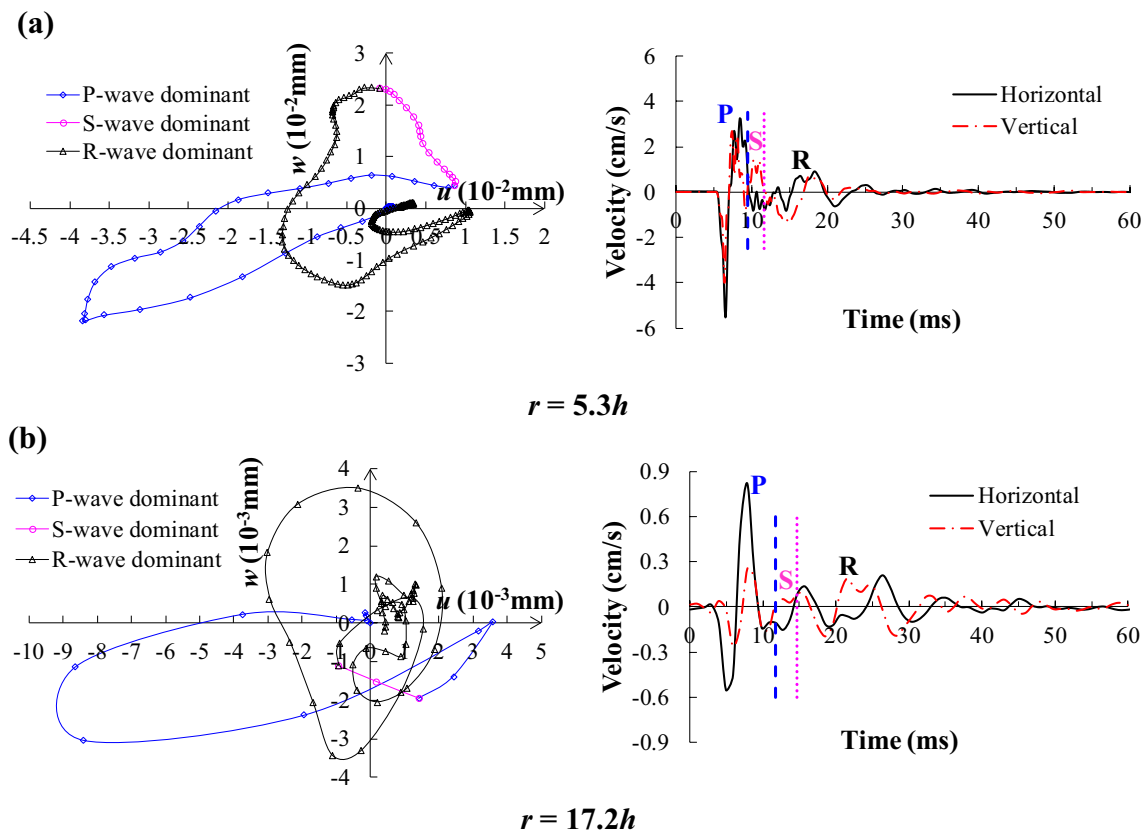
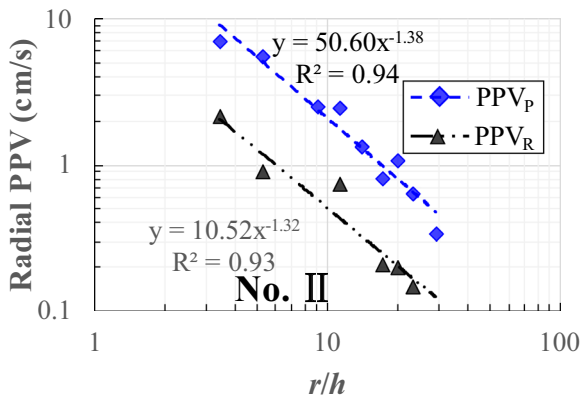


Fig. 17 Interpretation of the seismic components at the ground surface in Fengning pumped storage power station: **a** seismic waves at $r=5.3 h$; **b** Seismic waves at $r=17.2 h$

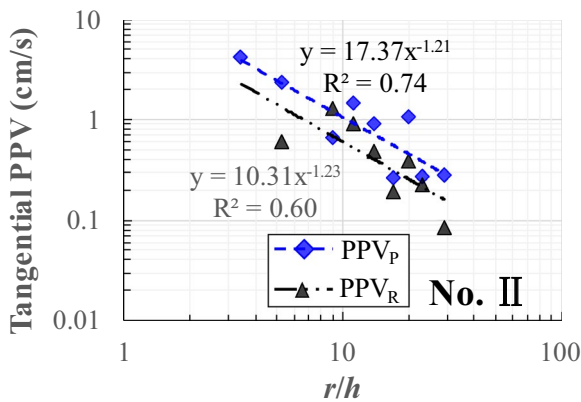
for example, the P-wave mainly dominates the horizontal vibration, and the R-wave grows gradually and dominates the vertical vibration in the far field. The detailed analysis of the evolution of various waves will be presented in the following section.

4.3.2 Evolution of P- and R-waves at the ground surface

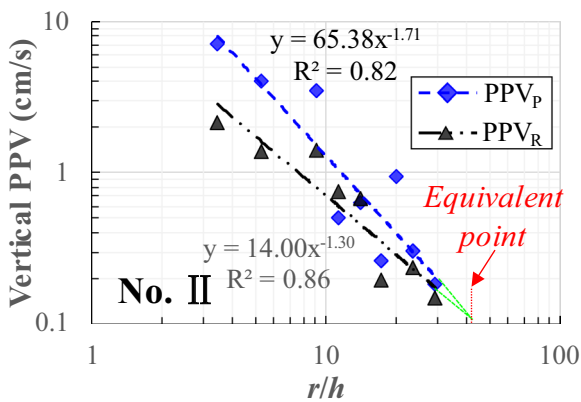
The PPV values associated with blastholes II, IV and VI are listed in (see Table 5 Appendix 1), where PPV_P and PPV_R are the PPV in P- and R-waves, respectively. Figures 18, 19, 20 plot the evolution of PPV with r/h at the



(a)

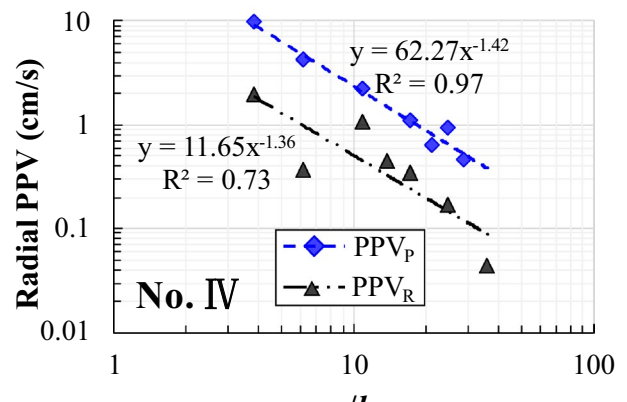


(b)

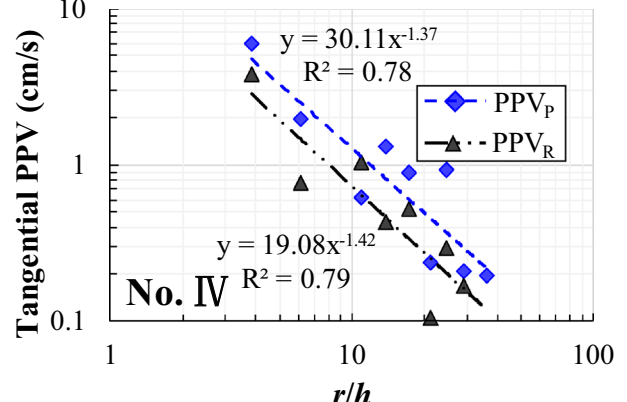


(c)

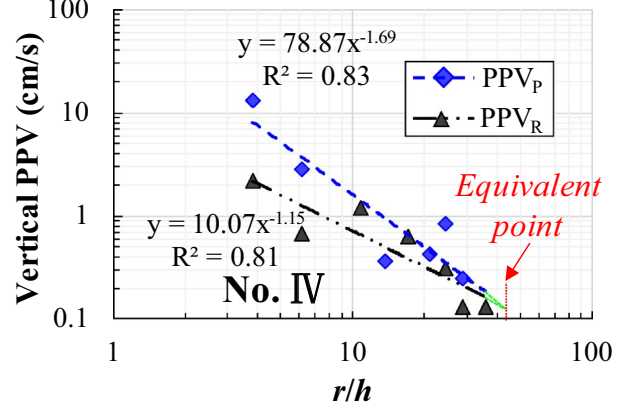
Fig. 18 Evolution of P- and R-waves induced by blasthole II, where the *Equivalent point* means that $PPV_P = PPV_R$, and PPV_P and PPV_R are the PPV in P- and R-waves, respectively: **a** horizontal radial PPV; **b** horizontal tangential PPV; **c** vertical PPV



(a)



(b)



(c)

Fig. 19 Evolution of P- and R-waves induced by blasthole IV, where the *Equivalent point* means that $PPV_P = PPV_R$, and PPV_P and PPV_R are the PPV in P- and R-waves, respectively: **a** horizontal radial PPV; **b** horizontal tangential PPV; **c** vertical PPV

ground surface, where r/h is defined as a dimensionless indicator to analyze the evolution of different waves in

this paper. As the recorded S-wave component is ignorable, only the P- and R-waves are included in the figure.

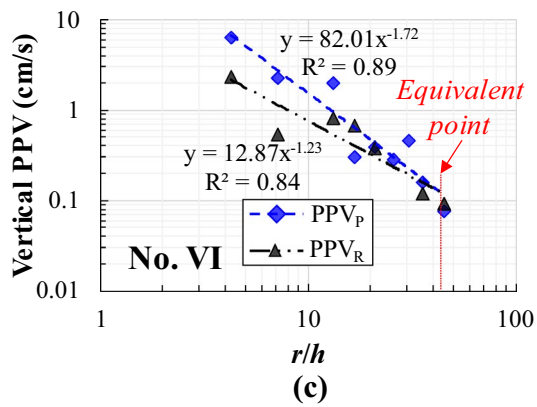
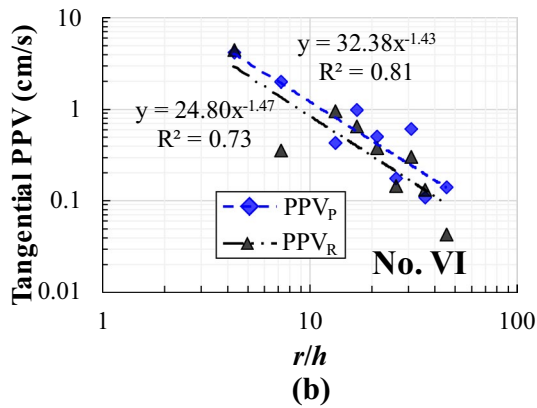
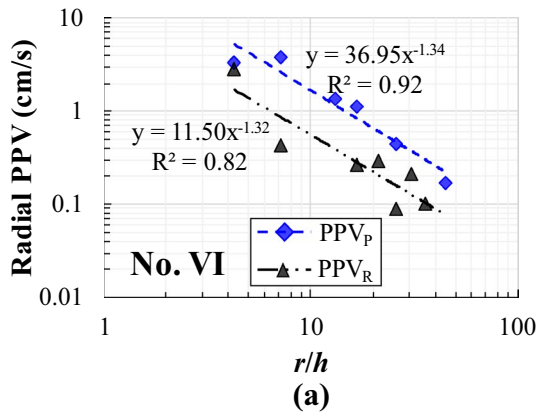


Fig. 20 Evolution of P- and R-waves induced by blasthole IV, where the Equivalent point means that $PPV_P = PPV_R$, and PPV_P and PPV_R are the PPV in P- and R-waves, respectively: **a** horizontal radial PPV; **b** horizontal tangential PPV; **c** vertical PPV

The relationship of PPV *versus* r/h are fitted by the power function, as expressed in Eq. (1).

$$PPV = K(r/h)^{-\alpha}, \tag{1}$$

Where K and α are both the attenuation coefficients associated with the wave type and onsite geology conditions.

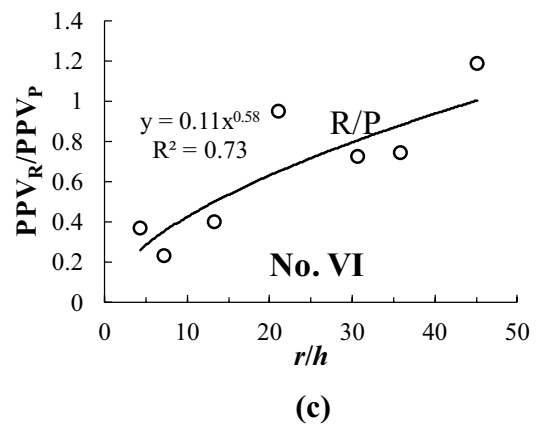
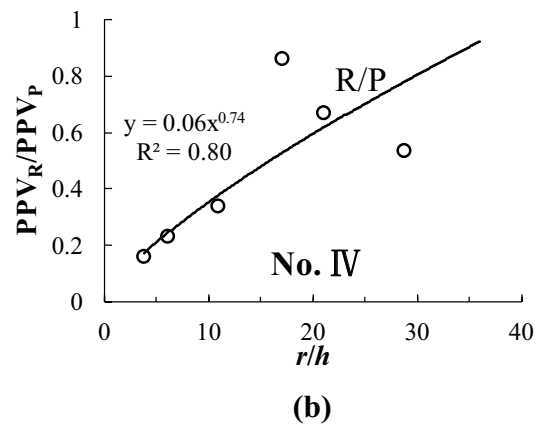
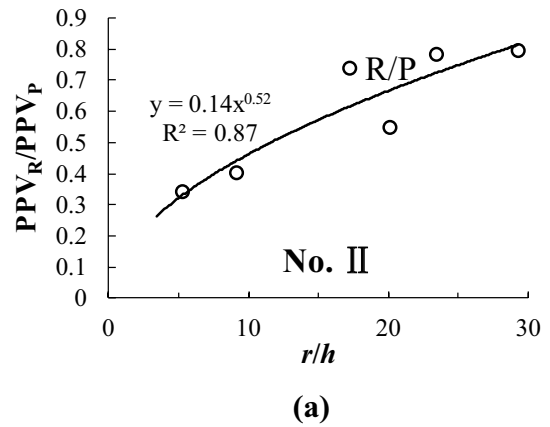


Fig. 21 Evolution of the vertical PPV_R/PPV_P at the ground surface, where PPV_P and PPV_R are the PPV in P- and R-waves, respectively: **a** PPV induced by blasthole II; **b** PPV induced by blasthole IV; **c** PPV induced by blasthole VI

Figures 18, 20 indicate that the evolutions of P- and R-waves with r significantly differ from each other. The horizontal radial and tangential PPV values in the P-wave are much higher than those in the R-wave, and the radial and tangential PPV decay speeds α slightly

Table 3 Predicted location of the *Equivalent point* of P- and R-waves in the vertical PPV

| Blasthole no. | Buried depth h (m) | Charge weight (kg) | P-wave | | R-wave | | Location of equivalent point | |
|---------------|----------------------|--------------------|--------|------------|--------|------------|------------------------------|---------------------|
| | | | K_P | α_P | K_R | α_R | r/h | SD ($m/kg^{1/2}$) |
| II | 5.0 | 12.0 | 65.38 | 1.71 | 14.00 | 1.30 | 42.9 | 61.9 |
| IV | 4.0 | 8.4 | 78.87 | 1.69 | 10.07 | 1.15 | 45.2 | 62.4 |
| IV | 3.15 | 5.4 | 82.01 | 1.72 | 12.87 | 1.23 | 43.8 | 59.4 |

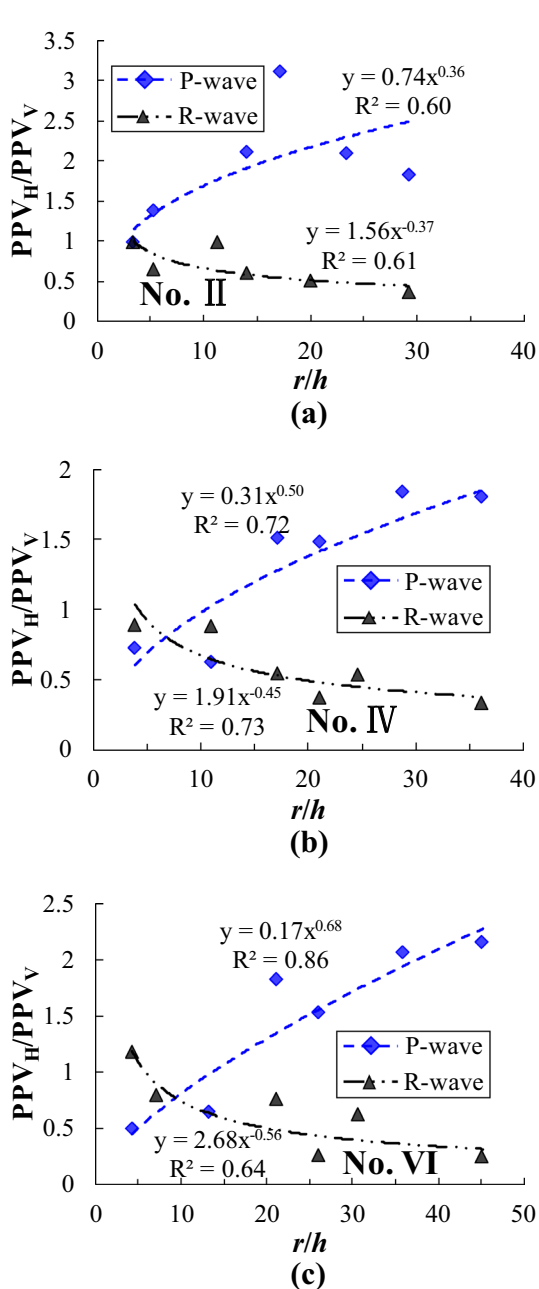


Fig. 22 Evolution of PPV_H/PPV_V at the ground surface, where PPV_H and PPV_V are the horizontal and vertical PPV, respectively: **a** PPV induced by blasthole II; **b** PPV induced by blasthole IV; **c** PPV induced by blasthole VI

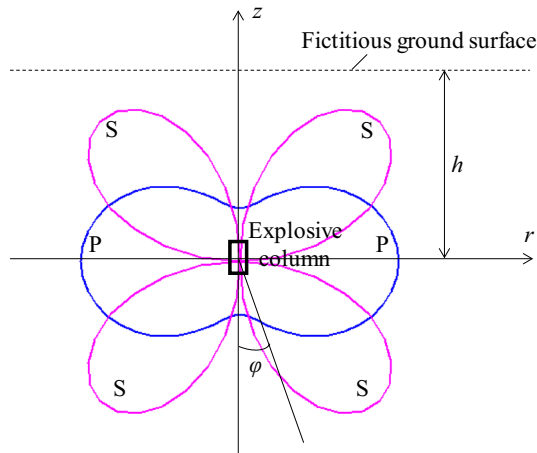


Fig. 23 Source radiation pattern of a short explosive column (Heelan 1953)

vary for P- and R-waves. Thus, the P-wave is a significant component in both near and far fields. However, for the vertical PPV, the R-wave has a slower decay speed than P-wave, since the decay factor in the R-wave is 0.41–0.54 less than that in the P-wave. The vertical PPV_R/PPV_P ratio versus r/h is plotted in Fig. 21, which shows that the PPV_R/PPV_P ratio is an increasing indicator. The location of the Equivalent point can be predicted by solving Eq. (2), and the solution is expressed as Eq. (3).

$$K_P(r/h)^{-\alpha_P} = K_R(r/h)^{-\alpha_R}, \tag{2}$$

$$(r/h) = (K_P/K_R)^{1/(\alpha_P-\alpha_R)}, \tag{3}$$

Where K_P , K_R , α_P and α_R are the attenuation coefficients of P- and R-waves, respectively. As the charge weight scaling law is widely used in the prediction of blast vibration, the location of the Equivalent point is also predicted in the form of SD (Scaled distance, $m/kg^{1/2}$). Table 3 lists the predicted location of the *Equivalent point* in the vertical PPV, which is also illustrated in Figs. 18, 20. The prediction results indicate that the R-wave dominates the vertical vibration if r exceeds $(43-45)h$, or SD exceeds 59–62 $m/kg^{1/2}$. The evolution of P- and R-waves also shows that the proportion

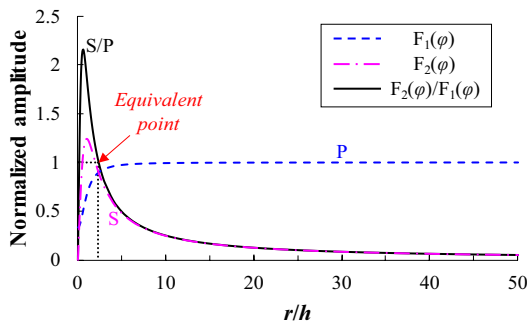


Fig. 24 Evolution of the source-radiated waves

of different seismic components varies with r , and the domi-

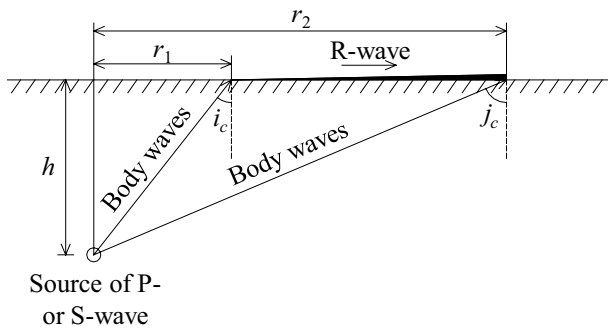


Fig. 25 Illustration of the generation range of the R-wave

nant wave may change to another type.

4.3.3 Evolution of PPV_H/PPV_V at the ground surface

Figure 22 shows the evolution of PPV_H/PPV_V at the ground surface, where PPV_H and PPV_V are the horizontal and vertical PPV, respectively. It indicates that the PPV_H/PPV_V ratio of the P-wave increases with r/h , while that of the R-wave is a decreasing curve. In other words, the particle motion of the P-wave gradually rotates to the horizontal direction, while the dominant motion of the ground R-wave lies in the vertical direction. The PPV_H/PPV_V ratio in the R-wave tends to be stable in the far field, which is identical with the nature of the R-wave, since whose vertical vibration is superior to the horizontal vibration at the ground surface. The analysis of the evolution of PPV_H/PPV_V also shows that the dominant motion directions of various waves are distinct.

5 Discussion

5.1 Evolution of source-radiated waves

The test results in the first case study shows that the PPV in the P-wave might be higher than that in the S-wave. This finding appears to contradict the claims of Blair (2015), who shows that the S-wave carries more energy than the P-wave in most cases. But we think that this contradiction is caused by the difference in descriptions of the problem: Blair (2015) focuses on the energy partition of source radiation, whereas the present study describes the evolution of various waves at different locations. As shown in Fig. 23, Heelan (1953) made a vital contribution to the source radiation pattern of a short explosive column. He declared that both P- and S-waves are of primary origins, which are simultaneously radiated from the explosive column. Figure 23 also indicates that both P- and S-waves channel in certain directions, and their amplitudes are respectively proportional to the source functions $F_1(\varphi)$ and $F_2(\varphi)$, as expressed in Eqs. (4) and (5). The P-wave dominates in the radial direction of the column, while the dominant orientation of the S-wave makes an angle of 45° with the column axis. Therefore, the proportion of P- and S-wave components certainly varies with the location or orientation of interest. Although the S-wave carries more energy from the source, the P-wave still can have a larger amplitude than the S-wave at a special location.

$$F_1(\varphi) = \frac{\Delta}{4\pi GV_P} \left(1 - \frac{2V_S^2}{V_P^2} \cos^2 \varphi \right) \tag{4}$$

$$F_2(\varphi) = \frac{\Delta}{4\pi GV_S} \sin(2\varphi), \tag{5}$$

where Δ is the volume of the equivalent column cavity, and φ is the angle between the radiation direction and blasthole axis.

For a vertical blasthole, the evolution of the source-radiated waves can be displayed by the source functions. Figure 24 plots the evolution of normalized source functions $F_1(\varphi)$ and $F_2(\varphi)$ with r at the fictitious ground surface (see Fig. 23). It indicates that the amplitude in the P-wave increases with r , while the source function of the S-wave is a decreasing curve. The amplitude ratio $F_2(\varphi)/F_1(\varphi)$ decreases rapidly with r , which implies that the effect of the S-wave is negligible in the far field. The P-wave becomes the dominant component when r exceeds $2.3h$. The S-wave only dominates the vibration within $r=2.3h$, where $F_2(\varphi)/F_1(\varphi)$ reduces to 1.0. Thus, the source radiation

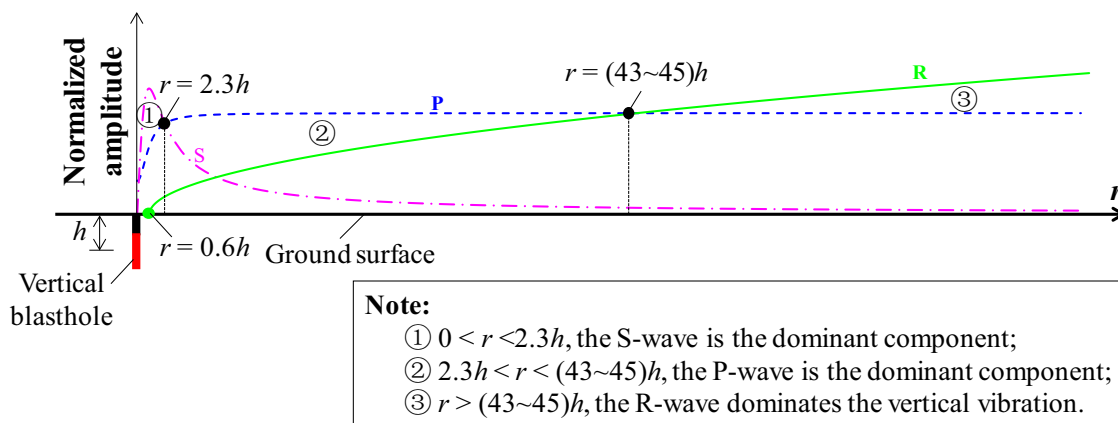


Fig. 26 Partition of the influence areas of various waves

pattern plays an important role in the evolution of different seismic waves.

5.2 Generation of the R-wave

For the generation of the R-wave under a buried source, Nakano (Kuzmenko et al 1993) and Aki et al. (2002) found that the R-wave is not suddenly created at the epicenter but forms entirely where $r > h$, and its origin is not precisely known. But they have proven that the generation range of the R-wave depends on the incident angle of body waves to the ground surface. The approximate angle to predict the position of origin can be ascertained by Eqs. (6) and (7). The critical angle to determine where the R-wave is well developed can be estimated by Eq. (8). Figure 25 illustrates of the generation range of the R-wave.

$$\tan i_c = \frac{r_1}{h} \geq \frac{C_R}{\sqrt{C_P^2 - C_R^2}}, \text{ for source of the P-wave} \quad (6)$$

$$\tan i_c = \frac{r_1}{h} \geq \frac{C_R}{\sqrt{C_S^2 - C_R^2}}, \text{ for source of the S-wave} \quad (7)$$

$$\tan j_c = \frac{r_2}{h} > \sqrt{\frac{2C_R}{C_S - C_R}}, \quad (8)$$

where, i_c is the critical angle that predicts the position of origin, j_c is the critical angle to determine the position where the R-wave is well developed, r_1 is the epicenter distance associated with i_c , r_2 is the epicenter distance

associated with j_c and h is the buried depth of the source. Because $C_P = \sqrt{3}C_S$ and $C_R \approx 0.92C_S$ for most rocks, the critical epicenter distance satisfies $r_1 \approx 0.6h$ and $r_2 \approx 5h$. The test results in the second case study also show that a small R-wave appears in the particle motion trajectories if $r < 5h$ (see Fig. 27 in Appendix 2), but it is easily found when $r > 5h$. In other words, unlike the source-radiated P- and S-waves, the R-wave is of secondary origin, which is generated by the wave reflection at the ground surface and gradually grows with r .

5.3 Partition of the influence areas of various waves

As was stated above, various waves have notably different evolution laws and influence areas. The proportion of different seismic components is not a constant, but rather, the dominant wave may change to another type with r , and the dominant motion directions of various waves are distinct. Figure 26 illustrates the partition of the influence areas of various waves according to the test results and the discussion in Sect. 5.2. For a vertical blasthole, the P-wave becomes the dominant component if $r > 2.3h$, and it mainly contributes to the horizontal vibration. The S-wave is the dominant component within $r = 2.3h$, but its effect can be ignored when the R-wave is well developed. The R-wave is not suddenly created but gradually grows with r , and it dominates the vertical vibration if r exceeds $(43\sim 45)h$. The two factors, including the source radiation pattern and the physical damping along the travel path, both play an important role in the evolution of various waves. However, the present partition of the influence areas merely results from two case studies. More onsite experiments are required in the next stage.

Figure 26 implies that the P-wave is a non-negligible threat to ground structures in vertical-hole blasting. However, the P-wave component is commonly ignored in earthquakes, where the S- and R-waves are considered troublesome. This contradiction is caused by the differences in the source pattern and source-to-site distance scale. On one hand, an earthquake is caused by the shear fracture of the rock plate, so the seismic source is actually a shear source. But blasting is a type of dilatation source because the explosion energy is transmitted to the rock mass by the expansion of gaseous detonation products. On the other hand, the location of interest in blasting operations is usually close to the explosion source, while the receivers in seismology are tens or hundreds of kilometers away from the earthquake source. Therefore, the evolution of seismic components induced by blasting has some differences from the expectations in earthquakes.

6 Conclusions

This paper is an attempt to analyze the evolution of seismic components induced by a vertical blasthole, and the partition of the influence areas of various waves was preliminarily discussed. The present study allows the following conclusions:

1. The evolution of various waves and their influence areas are notably different. The proportion of different seismic components is not a constant, but rather, the dominant wave may change to another type with r , and the dominant motion directions of various waves are distinct.
2. For a vertical blasthole, the P-wave is a significant component in both near and far fields, and becomes the dominant wave beyond $r = 2.3 h$, furthermore its particle motion gradually rotates to the horizontal direction with r increases. The S-wave only dominates within $r = 2.3 h$, but its effect can be ignored when the R-wave is well developed. The R-wave is not suddenly created but gradually grows to an identifiable feature at $r = 5 h$, and it dominates the vertical vibration if r exceeds $(43-45)h$ ($59-62 \text{ m/kg}^{1/2}$).
3. The P-wave is a non-negligible threat to ground structures in vertical-hole blasting. However, the P-wave component is commonly ignored in earthquakes, where the S- and R-waves are considered troublesome. The evolution of seismic components induced by blasting has some differences from the expectations in earthquakes.

We merely analyzed the evolution of seismic components induced by a vertical blasthole. The seismic waves induced by other blasting sources or the blasting operations with more complex boundary conditions will be studied in the future. The thorough separation of different waves will also be covered in the next stage, so as to further reveal the characteristic of each seismic component.

Acknowledgements This work is supported by the National Natural Science Fund Project of China (51779190) and Hubei Province Technical Innovation Program (2017ACA102). The authors wish to express their thanks to all supporters.

Appendix 1

See Tables 4 and 5.

Table 4 PPV within rock mass in Baihetan hydropower station

| Blasthole no. | Geophone no. | PPV _P (cm/s) | | PPV _S (cm/s) | |
|---------------|--------------|-------------------------|----------|-------------------------|----------|
| | | Horizontal | Vertical | Horizontal | Vertical |
| A | 1# | 16.72 | 7.95 | 1.02 | 3.80 |
| | 2# | 0.53 | 0.61 | 0.17 | 0.36 |
| B | 1# | 29.29 | 9.01 | 2.96 | 3.59 |
| | 2# | 3.57 | 1.51 | 0.86 | 1.27 |
| C | 1# | 36.50 | 36.50 | 4.73 | 24.1 |
| | 2# | 1.25 | 1.25 | 0.30 | 0.82 |
| D | 1# | 36.50 | 36.50 | 4.76 | 27.56 |
| | 2# | 2.75 | 3.21 | 0.67 | 1.30 |

Table 5 PPV at the ground surface in Fengning pumped storage power station

| Blasthole no. | Geophone no. | PPV _p (cm/s) | | | PPV _R (cm/s) | | |
|---------------|--------------|-------------------------|------------|----------|-------------------------|------------|----------|
| | | Radial | Tangential | Vertical | Radial | Tangential | Vertical |
| II | 1# | 7.02 | 4.16 | 7.10 | 2.15 | 4.84 | 2.16 |
| | 2# | 5.54 | 2.36 | 3.99 | 0.90 | 0.60 | 1.36 |
| | 3# | 2.53 | 0.66 | 3.49 | 1.59 | 1.30 | 1.41 |
| | 4# | 2.49 | 1.46 | 0.50 | 0.74 | 0.90 | 0.75 |
| | 5# | 1.35 | 0.91 | 0.64 | 0.40 | 0.49 | 0.67 |
| | 6# | 0.82 | 0.26 | 0.26 | 0.21 | 0.20 | 0.20 |
| | 7# | 1.09 | 1.08 | 0.94 | 0.20 | 0.39 | 0.39 |
| | 8# | 0.63 | 0.27 | 0.30 | 0.15 | 0.23 | 0.24 |
| | 9# | 0.34 | 0.28 | 0.18 | 0.05 | 0.08 | 0.15 |
| IV | 1# | 9.68 | 5.99 | 13.25 | 1.95 | 3.84 | 2.18 |
| | 2# | 4.28 | 1.97 | 2.85 | 0.37 | 0.76 | 0.67 |
| | 3# | 2.20 | 0.61 | 3.50 | 1.06 | 1.03 | 1.20 |
| | 4# | 2.21 | 1.29 | 0.36 | 0.45 | 0.43 | 0.41 |
| | 5# | 1.10 | 0.89 | 0.73 | 0.34 | 0.52 | 0.63 |
| | 6# | 0.64 | 0.24 | 0.43 | 0.11 | 0.11 | 0.29 |
| | 7# | 0.93 | 0.93 | 0.84 | 0.17 | 0.30 | 0.32 |
| | 8# | 0.45 | 0.21 | 0.25 | 0.10 | 0.17 | 0.13 |
| | 9# | 0.24 | 0.20 | 0.13 | 0.04 | 0.06 | 0.13 |
| VI | 1# | 3.25 | 4.20 | 6.41 | 2.81 | 4.48 | 2.37 |
| | 2# | 3.79 | 2.02 | 2.30 | 0.43 | 0.36 | 0.54 |
| | 3# | 1.32 | 0.43 | 2.03 | 0.85 | 0.97 | 0.82 |
| | 4# | 1.10 | 0.99 | 0.30 | 0.26 | 0.67 | 0.67 |
| | 5# | 0.73 | 0.51 | 0.40 | 0.29 | 0.38 | 0.38 |
| | 6# | 0.44 | 0.18 | 0.29 | 0.09 | 0.15 | 0.34 |
| | 7# | 0.60 | 0.63 | 0.47 | 0.21 | 0.31 | 0.34 |
| | 8# | 0.34 | 0.11 | 0.16 | 0.10 | 0.13 | 0.12 |
| | 9# | 0.17 | 0.14 | 0.08 | 0.02 | 0.04 | 0.09 |

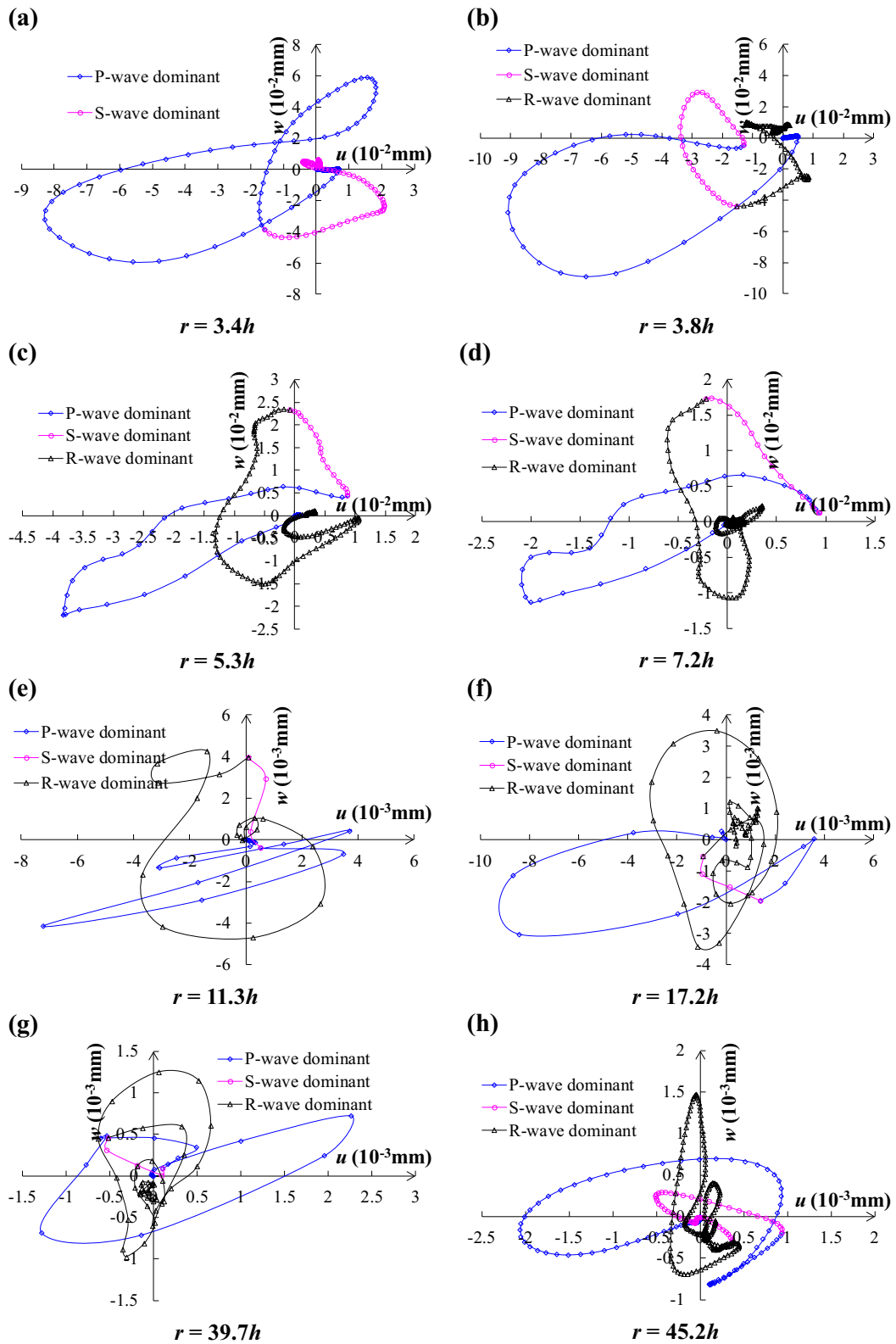


Fig. 27 Particle motion trajectories at the ground surface in Fengning pumped storage station

Appendix 2

See Fig. 27.

References

- Abo-Zena AM (1977) Radiation from a finite cylindrical explosive source. *Geophysics* 42(7):1384–1393
- Achenbach JD (1973) *Wave propagation in elastic solids*. North-Holland Publishing, New York
- Aki K, Richards PG (2002) *Quantitative Seismology*, 2nd edn. University Science Books, Sausalito
- Álvarez-Vigil AE, González-Nicieza C, Gayarre FL, Álvarez-Fernández MI (2012) Predicting blasting propagation velocity and vibration frequency using artificial neural networks. *Int J Rock Mech Min Sci* 55(10):108–116
- Blair DP (1993) Polarization analysis of seismic events. Report to Kalgoorlie Consolidated Goldmines (KCGM)
- Blair DP (2007) A comparison of Heelan and exact solutions for seismic radiation from a short cylindrical charge. *Geophysics* 72(2):E33–E41
- Blair DP (2010) Seismic radiation from an explosive column. *Geophysics* 75(1):E55–E65
- Blair DP (2011a) A probabilistic analysis of vibration based on measured data and charge weight scaling. In: *Proceedings of the 6th EFEE world conference on explosives and blasting technique*, Lisbon, Portugal, pp 319–337
- Blair DP (2015) The free surface influence on blast vibration. *Int J Rock Mech Min Sci* 77:182–191
- Blair DP, Minchinton A (1996) On the damage zone surrounding a single blasthole. In: *Proceedings of the 5th international symposium on rock fragmentation by blasting*. Balkema, Rotterdam, pp 121–130
- Bott MHP (1982) *The Interior of the Earth, Its Structure Constitution and Evolution*, 2nd edn. Edward Arnold, London
- Dowding CH (1985) *Blast vibration monitoring and control*, vol 297. Prentice-Hall, Englewood Cliffs
- Dowding CH (1996) *Construction vibrations*, vol 610. Prentice Hall, Upper Saddle River
- Favreau RF (1969) Generation of strain waves in rock by an explosion in a spherical cavity. *J Geophys Res* 74(17):4267–4280
- Gao Q, Lu W, Hu Y, Yang Z, Yan P, Chen M (2017) An evaluation of numerical approaches for S-wave component simulation in rock blasting. *J Rock Mech Geotech Eng* 9(5):830–842
- Graff KF (1975) *Wave motion in elastic solid*
- Hagan TN (1979) Rock breakage by explosives. *Acta Astronaut* 6:329–340
- Hao H, Wu Y, Ma G, Zhou Y (2001) Characteristics of surface ground motions induced by blasts in jointed rock mass. *Soil Dyn Earthq Eng* 21(2):85–98
- Heelan PA (1953) Radiation from a cylindrical source of finite length. *Geophysics* 18(3):685
- Jordan DW (1962) The stress wave from a finite, cylindrical explosive source. *J Appl Math Mech* 11(4):503–551
- Khandelwal M (2010) Evaluation and prediction of blast-induced ground vibration using support vector machine. *Int J Rock Mech Min Sci* 47(3):509–516
- Khandelwal M, Singh TN (2007) Evaluation of blasting induced ground vibration predictors. *Soil Dyn Earthq Eng* 27:116–125
- Khandelwal M, Singh TN (2009) Prediction of blast-induced ground vibration using artificial neural network. *Int J Rock Mech Min Sci* 46(7):1214–1222
- Khandelwal M, Singh TN (2013) Application of an expert system to predict maximum explosive charge used per delay in surface mining. *Rock Mech Rock Eng* 46(6):1551–1558
- Kuzmenko AA, Vorobev VD, Denisjuk II, Dauetas AA (1993) Seismic effects of blasting in rock
- Kuzu C (2008) The importance of site-specific characters in prediction models for blast-induced ground vibrations. *Soil Dyn Earthq Eng* 28(5):405–414
- Ozer U (2008) Environmental impacts of ground vibration induced by blasting at different rock units on the Kadikoy–Kartal metro tunnel. *Eng Geol* 100(1–2):82–90
- Park J, Vernon FL, Lindberg CR (1987) Frequency dependent polarization analysis of high-frequency seismograms. *J Geophys Res* 92(B12):12664–12674
- Singh PK, Roy MP (2010) Damage to surface structures due to blast vibration. *Int J Rock Mech Min Sci* 47(6):949–961
- Singh PK, Mohanty B, Roy MP (2008) Low frequency vibrations produced by coal mine blasting and their impact on structures. *Int J Blast Fragm* 2(1):71–89
- Triviño LF, Mohanty B, Munjiza A (2009) Seismic radiation patterns from cylindrical explosive charges by combined analytical and combined finite-discrete element methods. *Fragblast* 13:415–426
- Triviño LF, Mohanty B, Milkereit B (2012) Seismic waveforms from explosive sources located in boreholes and initiated in different directions. *J Appl Geophys* 87:81–93
- Vanbrabant F, Chacon E, Quinones L (2002) P and S Mach waves generated by the detonation of a cylindrical explosive charge - Experiments and simulations. *Fragblast* 6(1):21–35
- Verma AK, Singh TN (2013) Comparative study of cognitive systems for ground vibration measurements. *Neural Comput Appl* 22(Suppl. 1):341–350
- Vidale JE (1986) Complex polarization analysis of particle motion. *Bull Seism Soc Am* 76(5):1393–1405
- White JE (1983) *Underground sound: application of seismic waves*. Elsevier, Amsterdam
- Whitham GB (1999) *Linear and nonlinear waves*. Wiley, New York
- Yan WM, Yuen KV (2015) On the proper estimation of the confidence interval for the design formula of blast-induced vibrations with site records. *Rock Mech Rock Eng* 48(1):361–374
- Yang J, Lu W, Jiang Q, Yao C, Jiang S, Tian L (2016) A study on the vibration frequency of blasting excavation in highly stressed rock masses. *Rock Mech Rock Eng* 49(7):2825–2843
- Yi C, Johansson D, Nyberg U, Beyglou A (2016) Stress wave interaction between two adjacent blast holes. *Rock Mech Rock Eng* 49(5):1803–1812
- Zhou J, Lu W, Yan P, Chen M, Wang G (2016) Frequency-dependent attenuation of blasting vibration waves. *Rock Mech Rock Eng* 49:1–12

Publisher's Note Springer Nature remains neutral with regard to jurisdictional claims in published maps and institutional affiliations.